

TIDAL DWARF GALAXIES AROUND A POST-MERGER GALAXY, NGC 4922

Yun-Kyeong Sheen¹, Hyunjin Jeong¹, Sukyoung K. Yi^{1*}, Ignacio Ferreras², Jennifer M. Lotz³, Knut A. G. Olsen³, Mark Dickinson³, Sydney Barnes⁴, Jang-Hyun Park⁵, Chang H. Ree⁵, Barry F. Madore⁶, Tom A. Barlow⁷, Tim Conrow⁷, Karl Foster⁷, Peter G. Friendman⁷, Young-Wook Lee¹, D. Christopher Martin⁷, Patrick Morrissey⁷, Susan G. Neff⁸, David Schiminovich⁹, Mark Seibert⁶, Todd Small⁷, Ted K. Wyder⁷
 yi@yonsei.ac.kr

ABSTRACT

One possible channel for the formation of dwarf galaxies involves birth in the tidal tails of interacting galaxies. We report the detection of a bright UV tidal tail and several young tidal dwarf galaxy (TDG) candidates in the post-merger galaxy NGC 4922 in the Coma cluster. Based on a two-component population model (combining young and old stellar populations), we find that the light of tidal tail predominantly comes from young stars (a few Myr old). The *Galaxy Evolution Explorer* (*GALEX*) ultraviolet data played a critical role in the parameter (age and mass) estimation. Our stellar mass estimates of the TDG candidates are $\sim 10^{6-7} M_{\odot}$, typical for dwarf galaxies.

Subject headings: galaxies: dwarf – galaxies: individual(NGC 4922) – galaxies: interactions – galaxies: starburst – ultraviolet: galaxies

1. INTRODUCTION

A tidal dwarf galaxy (hereafter TDG) is defined as “a dwarf-sized self-gravitating object assembled from tidal debris” (Hibbard et al. 2005).

¹Department of Astronomy, Yonsei University, Seoul 120-749, Republic of Korea

²Mullard Space Science Laboratory, University College London, Holmbury St Mary, Dorking, Surrey, RH5 6NT, UK

³National Optical Astronomy Observatory, 950 North Cherry Avenue, Tucson, AZ 85719, USA

⁴Lowell Observatory, Flagstaff, AZ 86001, USA

⁵Korea Astronomy and Space Science Institute, Hwaam 61-1, Yuseong, Daejeon 305-348, Republic of Korea

⁶Observatories of the Carnegie Institution of Washington, 813 Santa Barbara St., Pasadena, CA 91101, USA

⁷California Institute of Technology, MC 405-47, 1200 E. California Blvd., Pasadena, CA 91125, USA

⁸Laboratory for Astronomy and Solar Physics, NASA Goddard Space Flight Center, Greenbelt, MD 20771, USA

⁹Department of Astronomy, Columbia University, New York, NY 10027, USA

The formation of dwarf galaxies from tidal interactions was already suggested by Zwicky (1956). Two decades later, blue sources were found in the tidal tail of NGC 4038/39 (“the Antennae”), as well as HI tails in several other interacting galaxies (Schweizer 1978). In the 1990s, more TDGs were discovered (Schombert et al. 1990; Mirabel, Lutz & Maza 1991; Mirabel, Dottori & Lutz 1992). During the last two decades, about 20 more interacting galaxies and galaxy groups were investigated for the formation of TDGs (Hibbard et al. 1994; Yoshida, Taniguchi & Murayama 1994; Duc et al. 1997; Duc & Mirabel 1998; Duc et al. 2000; Heithausen & Walter 2000; Weilbacher et al. 2000; Hibbard et al. 2001; Mendes de Oliveira et al. 2001; Weilbacher, Duc & Fritze-v. Alvensleben 2003; Temporin et al. 2003; Mundell et al. 2004; Hibbard et al. 2005; Neff et al. 2005; Boquien et al. 2007, 2009; Hancock et al. 2009; Koribalski & López-Sánchez 2009; Smith et al. 2009; Konstantopoulos 2009). TDGs were found to feature blue optical colors revealing the existence of young stellar populations.

They are found at the tip of tidal tails, which usually correlates with H I gas density peaks. They also show higher metallicity than typical dwarf spheroidal galaxies, as expected, since they are assembled from recycled materials ejected by their merging parents.

The formation of tidal tails during the encounter of disk galaxies has been reproduced by numerical simulations (e.g., Toomre & Toomre 1972; Barnes 1988; Wetzstein et al. 2007). Wallin (1990) explored the triggering of star formation in tidal tails by combining a dynamical model with a code tracking the color evolution. Soon after, more detailed numerical simulations of the formation of dwarf galaxies in tidal tails followed (Barnes & Hernquist 1992; Elmegreen, Kaufman & Thomasson 1993). More recent simulations achieve much higher resolutions and include chemical evolution (e.g., Bournaud et al. 2008; Recchi et al. 2007). For instance, Bournaud et al. (2008) achieve resolutions high enough to probe down to the masses of star clusters ($\gtrsim 10^5 M_\odot$).

Nevertheless, much debate still exists on the fraction of dwarf galaxies born from tidal interactions, because it is difficult to identify TDGs once the tidal tail fades away. We can only identify TDGs by the presence of tidal tails or by a spectroscopic survey around galaxy mergers. Within the standard hierarchical formation scenario, fewer young tidal dwarf galaxies should be expected at present, compared to higher redshifts. Consequently, the number of confirmed TDGs is too small to characterize the population or to provide information for numerical studies.

Here, we focus on the formation of TDGs in the tidal tail of NGC 4922. NGC 4922 ($M_r = -22.1$, $z \sim 0.0235$) is a post-merger galaxy located at the outskirts of the Coma cluster. It is known as a merger between an early-type galaxy and a spiral galaxy. Two nuclei from its progenitors can be resolved, separated by ~ 10 kpc. This galaxy is especially interesting because the northern nucleus is a weak active galactic nucleus (AGN), probably as a consequence of the merging event. Andreasyan & Khachikyan (1986) and Alonso-Herrero et al. (1999) identified the northern nucleus as a Seyfert 2 galaxy with low ionization level. Alonso-Herrero et al. (1999) also showed the extended soft X-ray emission which did

not originate from the AGN, and possibly relates to ongoing star formation.

In this paper, we present and discuss a UV-bright tidal tail of NGC 4922 and TDG candidates obtained from data taken by the *Galaxy Evolution Explorer* (*GALEX*). In Section 2, we describe the *GALEX* observations and data reduction with supporting optical imaging and data reduction. In Section 3, we present the synthetic stellar population modeling. Star formation histories on the tidal tail and the TDG candidates are quantified and discussed in Section 4. We summarize our findings in Section 5.

2. OBSERVATIONS AND DATA REDUCTION

NGC 4922 is included in the Sloan Digital Sky Survey (SDSS; York et al. 2000). The typical exposure time for all SDSS u , g , r , i , and z bands is 53.9 s and the pixel scale is $0''.396 \text{ pixel}^{-1}$. We determined FWHM in each band using the `psfmeasure` task in Image Reduction and Analysis Facility (IRAF), as $1''.28$ for u , $1''.28$ for g , $1''.09$ for r , $1''.05$ for i and $0''.97$ for z band.

In order to explore faint features produced through the tidal interaction, we carried out optical deep imaging of NGC 4922 at Lowell Observatory. Observations were performed on 2007 April 16 with the Perkins Re-Imaging System (PRISM) mounted on the Perkins 1.8 m telescope. The field of view of the CCD is $13'.3 \times 13'.3$ and the pixel scale is $0''.390 \text{ pixel}^{-1}$. Images were taken in the V band and reduced using IRAF. In order to see faint structures around NGC 4922, one 30 minute exposure and two 20 minute exposures were combined in the V band. We followed the usual procedure for calibration using standard stars observed in the same night. The FWHM of the combined image is $2''.88$, also obtained via the `psfmeasure` task.

We used the *GALEX* public data of NGC 4922, taken between 2005 and 2006 in both the FUV (1350–1750 Å) and NUV (1750–2750 Å) bands. The data were acquired through the *GALEX* guest investigation project of Giuseppe Gavazzi (*G11-039006_Coma_MOS06*; Cortese, Gavazzi, & Boselli 2008). Details of the *GALEX* instruments, pipeline and calibration are described in Martin et al. (2005) and Morrissey et al. (2007). Total expo-

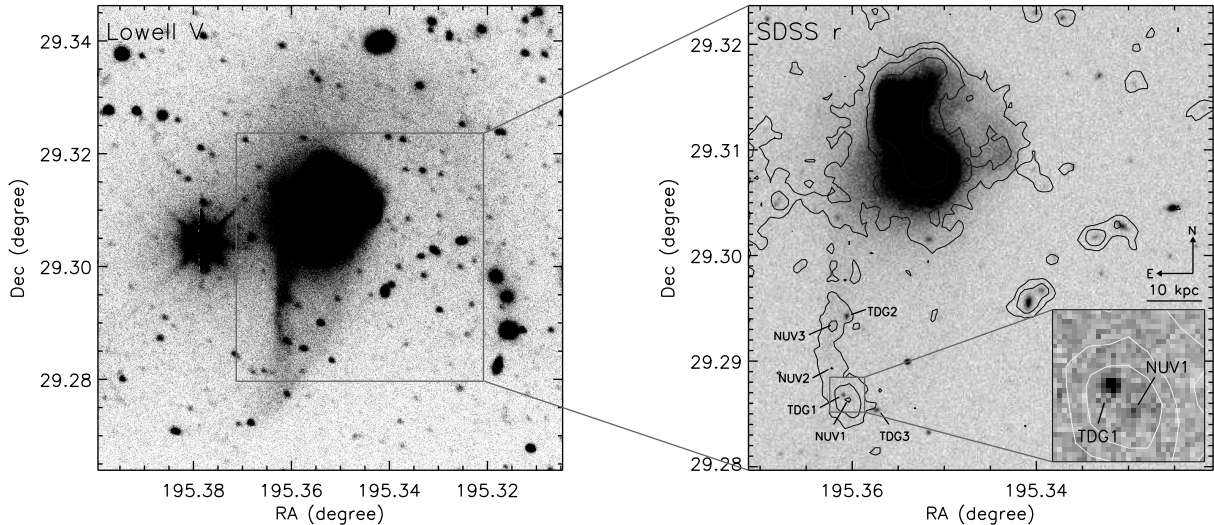


Fig. 1.— Left: optical V band deep image taken at Lowell Observatory. In addition to the UV-bright tidal tail, we can see faint tidal structures around NGC 4922. Right: *GALEX* NUV surface brightness contours are imposed over the optical SDSS r band image. Optical objects and NUV peaks are indicated and contours are given for $\mu_{\text{NUV}} \sim 26.0, 27.0, 28.0$ mag/arcsec². The inset shows optical counterparts of ‘TDG1’ and ‘NUV1’ in the SDSS r band. Contours are drawn for $\mu_{\text{NUV}} \sim 26.5, 27.0, 28.0$ mag/arcsec² in this case to see the faint object corresponding to ‘NUV1’. Because of the poor resolution of the *GALEX* data, we could not deblend the NUV light into the two optical objects.

sure times were 1693 s and 3524 s in FUV and NUV, respectively. The spatial resolution of the images are approximately $4''.2$ and $5''.3$ FWHM in FUV and NUV, respectively, sampled with $1''.5 \times 1''.5$ pixels.

Figure 1 shows the optical images with UV magnitude contours. The V -band deep image in the left panel reveals faint structures around NGC 4922 to the north and south of the galaxy. Along the tidal tail, the stellar debris of the interaction are visible. The right panel shows the shallower SDSS r -band image over which the NUV surface brightness contours are superimposed for $\mu_{\text{NUV}} = 26.0, 27.0, 28.0$ mag/arcsec². ‘TDG1’ and ‘NUV1’ are zoomed in in the inset image of the right panel with the NUV surface brightness contours for $\mu_{\text{NUV}} = 26.5, 27.0, 28.0$ mag/arcsec².

The apparent magnitudes are taken from the AUTO magnitudes measured by SExtractor (Bertin & Arnouts 1996). All UV and optical magnitudes in this study are measured in AB magnitude system. Galactic extinc-

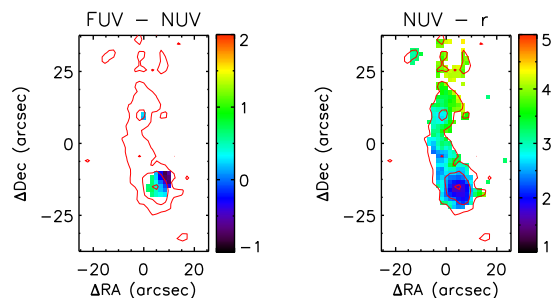


Fig. 2.— Color maps derived from the pixel magnitude maps of the tidal tail region. $S/N_{\text{FUV}} > 1$ cut is applied for ‘FUV–NUV’ color map while $S/N_{\text{NUV}} > 1$ cut is used for ‘NUV – r ’ color map. These maps show blue diagnostic colors indicating the presence of young stellar populations along the tidal tail.

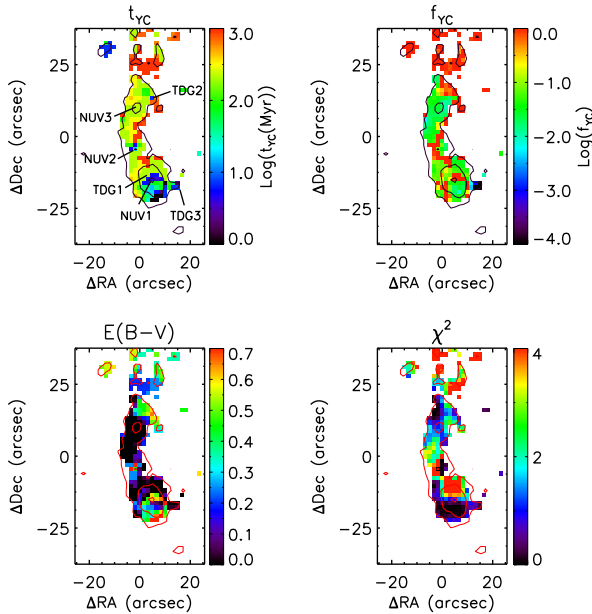


Fig. 3.— Predictions of the pixel-by-pixel analysis with two-component modeling in the tidal tail region. Only pixels of $S/N_{\text{NUV}} > 1$ and $\chi^2 < 4$ are presented. NUV surface brightness contours are given for $\mu_{\text{NUV}} = 26, 27, 28$ mag/arcsec². Clockwise from upper left, each panel shows the age of the young component in units of Myr, the young stellar mass fraction, χ^2 , and the internal extinction in $E(B - V)$.

tion was corrected using the reddening maps of Schlegel, Finkbeiner & Davis (1998) and the extinction law of Cardelli, Clayton & Mathis (1989). The extinctions for the *GALEX* passbands are $A_{\text{FUV}} = 8.24 \times E(B - V)$ and $A_{\text{NUV}} = 8.24 \times E(B - V) - 0.67 \times E(B - V)^2$ (Ree et al. 2007). Our photometric errors include photon-statistic errors as well as the flat-field variations of the UV data. In optical data, dark current and sky background were considered in the error budget.

In order to avoid spurious color gradients in the pixel-by-pixel analysis, caused by the different point-spread functions, we convolved the UV and optical data to a common FWHM of 6'' using the circular Gaussian kernel of `gauss` task in IRAF.

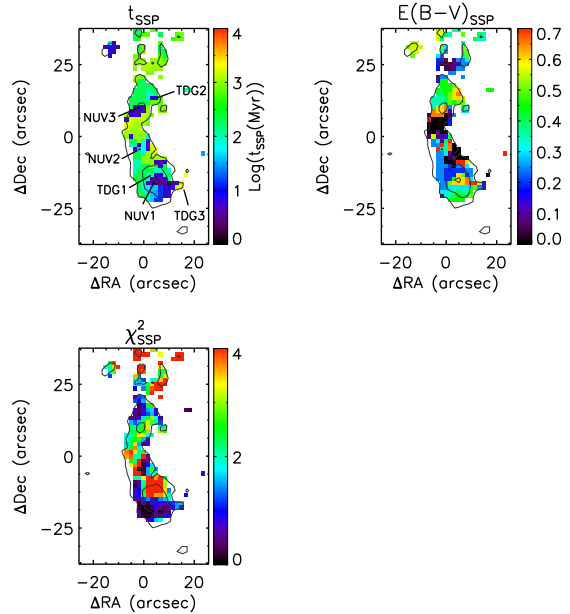


Fig. 4.— Results from SSP modeling of the pixel fluxes in the tidal tail region. Only pixels of $S/N_{\text{NUV}} > 1$ and $\chi^2 < 4$ are presented. NUV surface brightness contours are shown at the $\mu_{\text{NUV}} = 26, 27, 28$ mag/arcsec².

3. STELLAR POPULATION MODELING

The main focus of this paper is the study of the underlying stellar populations in the tidal tail of NGC 4922, using *GALEX* UV and SDSS optical data. Recent star formation is modeled by a superposition of an old and a young stellar component, following previous works (see e.g. Ferreras & Silk 2000; Yi et al. 2005; Kaviraj et al. 2007). The model takes two simple stellar populations (SSPs), whereby the free parameters are the age of the old and young components (t_{OC} and t_{YC} , respectively), the young stellar mass fraction (f_{YC}), and internal extinction ($E(B - V)$). The models of Yi (2003) are used to describe the old populations (1–12 Gyr). The models are based on single stellar populations with a solar metallicity. Since those models do not cover ages younger than 1 Gyr, we combine them with the models of *Starburst99* (Leitherer et al. 1999) at the age

of 1 Gyr. The second burst has a solar metallicity too. Internal extinction is applied to the composite spectral energy distribution (SED) models. The extinction curve is taken from Calzetti (2001).

We construct a library of over half a million SEDs for a grid of two-component models at the redshift of NGC 4922 ($z = 0.0235$). The grid has dimension $12 \times 36 \times 38 \times 33$ for t_{OC} , t_{YC} , f_{YC} and $E(B-V)$, respectively. t_{OC} extends from 1 Gyr to 12 Gyr while t_{YC} ranges from 1 Myr to 900 Myr. The young mass fraction, f_{YC} , is explored over its full possible range, 0 through 1, and $E(B-V)$ spreads over 0.0 to 0.7. The grid points in the two-dimensional parameter space spanned by t_{YC} and f_{YC} was chosen with logarithmic spacings, and adapted to extract the maximum sensitivity from the photometry on the presence of young populations.

The photometric SEDs of the objects are compared with the SEDs in the library and the best fit is determined via a standard likelihood estimator. We also compare the observations with models of SSPs, i.e., assuming a single age and metallicity.

4. DISCUSSION

The multiband data enable us to derive the stellar contents of this system. Note in Figure 1 that the UV light along the tail is brightest in the farthest half of the (optical) tail. Furthermore, the brightest UV knot is found at the tip of the tail. It seems that star formation is more active in the outer regions of tidal tails. This finding is consistent with the observational evidence of TDGs at the tip of the tidal tail in the Antennae galaxy (NGC4038/39, Hibbard et al. 2005) as well as the theoretical predictions (e.g., Bournaud & Duc 2006).

We found three optical objects which appear to be related with the NUV surface brightness distribution along the tail. Optical sources around the tidal tail are indicated as “TDG1,” “TDG2,” and “TDG3.” However, note that none of them is located exactly at the peaks in the NUV light. Hence we label the three NUV peaks separately as “NUV1,” “NUV2,” and “NUV3.”

We follow two complementary approaches to determine the color distribution of the sources on the tidal tail. In Section 4.1, we present a pixel-by-pixel analysis, which avoids the ambiguity of

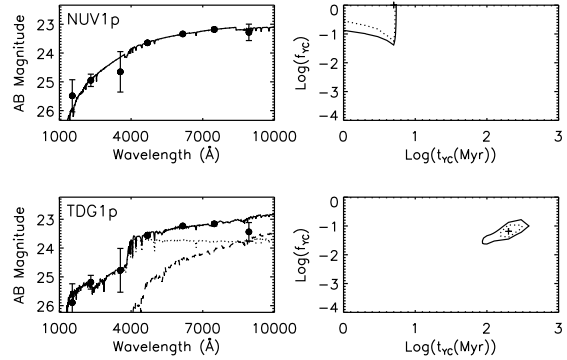


Fig. 5.— Best fit models from the pixel SEDs of “NUV1p” and “TDG1p” in the left panels. A dotted line shows the model SED of young component, while the dashed line indicates the contribution of an old component. In the right panels, χ^2 contours are presented for the 68% and 90% confidence levels (dashed and solid lines, respectively). A cross indicates the location where a minimum χ^2 was found in the parameter space. The best-fit values are presented in Table 1.

matching objects in UV and optical data. Furthermore, we consider aperture photometry of the targets, which increases the signal-to-noise ratio of the photometric data in Section 4.2.

4.1. Pixel-by-Pixel Analysis of the Tidal Tail Region

Figure 2 shows the “FUV – NUV” and “NUV – r ” color maps derived from pixel magnitude maps in the tidal tail region. Only the pixels with $S/N_{FUV} > 1$ are shown in “FUV – NUV” color map while the pixels with $S/N_{NUV} > 1$ are presented in “NUV – r ” color map. Surface brightness contours were superimposed on the color maps for $\mu_{NUV} = 26.0, 27.0, 28.0$ mag/arcsec². The tidal tail shows blue colors in both cases, suggesting the presence of stellar populations younger than 1 Gyr (NUV – $r \sim 4$ indicates a SSP of 1 Gyr at solar metallicity).

A photometric SED is constructed for each pixel using the pixel magnitude maps. Stellar population modeling was applied to the pixel SEDs according to the method described in Section 3. The

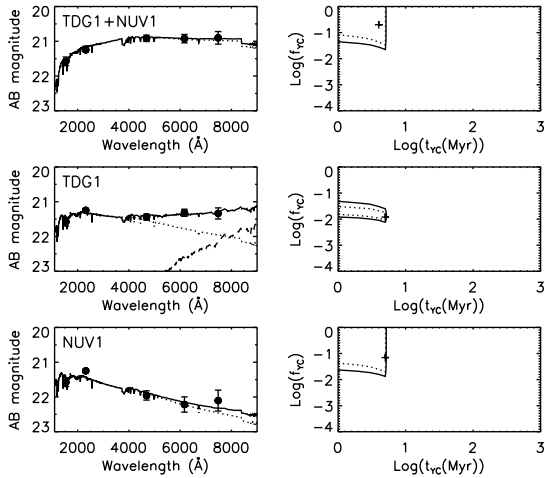


Fig. 6.— Result of stellar population modeling with SEDs derived from aperture photometry. Since we could not deblend the UV light around “TDG1” and “NUV1” into two separate sources, we add the optical SEDs from both objects. The upper panels show results for “TDG1+NUV1,” the middle panels are for the optical SED of “TDG1,” and the bottom panels are for “NUV1.” In the left panels dotted lines indicate the contribution of a young component while the dashed line shows a SED of an old component. In the right panels, χ^2 contours are presented for 68% and 90% confidence levels (dashed and solid lines, respectively). The result shows young populations of ~ 5 Myr.

results of the two-component (with $t_{OC} = 12\text{Gyr}$) and SSP modeling are presented in Figures 3 and 4. The result for the “central” pixel of each source is also presented in Table 1 (in order to avoid confusion between results using pixel SEDs and SEDs based on aperture photometry, we append a “p” at the end of their ID). The “central” pixel means a geometric center for TDG 1, 2, 3 and the NUV brightest pixel for NUV 1, 2, 3 actually. 1σ errors are presented in Table 1 also. They indicate that the age and internal extinctions are hardly defined in SSP modeling.

The results suggest that star formation has taken place along the tidal tail in the last few hundred Myr. The whole population of “NUV1p” is young, about 5 Myr old, with a large dust ex-

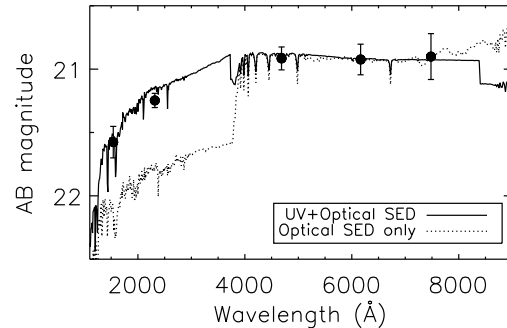


Fig. 7.— Best SSP model fits for “TDG1+NUV1.” The best fit is achieved for $t_{SSP} = 3$ Myr with the UV-optical SED, while it is 16 Myr when only the optical data are used to constrain the models (albeit with a large degeneracy). It shows the power of UV data to constrain the age derivation of young stellar populations.

inction. All other pixels, except “TDG3p”, also show significant mass fractions of young stars of 7–200 Myr old. Figure 5 shows the best model fits for “NUV1p” and “TDG1p”. χ^2 contours at the 68 and 90 percent confidence level are also presented in the right panels showing that parameters are reasonably well constrained by the data. The open contours of the confidence levels for the “NUV1p” source (top right panel) implies that an upper limit to the age of the young component (around 5 Myr) can be inferred. On the other hand, the two-component modeling of “TDG3p” shows a very low mass fraction in young stars (0.01 percent), and an old stellar population of a few Gyr for the SSP modeling. Considering that other parts of the tail are much younger, it is possible that “TDG3” is not associated with NGC 4922.

4.2. Aperture Photometry of TDG Candidates

We also carried out aperture photometry of the TDG candidates in the tidal tail in order to achieve a higher signal-to-noise ratio in their photometry. However, “TDG2” and “TDG3” do not have clear counterparts in the NUV images, they are just embedded in the extended UV structure. Therefore, we cannot apply aperture photometry

TABLE 1

PIXEL-BY-PIXEL MODELING RESULTS FOR THE CENTRAL PIXELS OF OUR 6 UV/OPTICAL SOURCES.

ID	$t_{YC,2CM}$ (Myr)	f_{YC} (%)	$E(B - V)_{2CM}$	t_{SSP} (Myr)	$E(B - V)_{SSP}$	RA(J2000) (hh:mm:ss)	Dec(J2000) (dd:mm:ss)
TDG1p	$200^{+110}_{-49.0}$	$6.5^{+4.3}_{-2.5}$	$0.^{+0.5}$	$100^{+143}_{-97.4}$	$0.19^{+0.48}_{-0.064}$	13:01:26.62	29:17:12.5
TDG2p	$7^{+0.02}_{-0.01}$	$4.5^{+9.6}_{-2.9}$	$0.6^{+0.02}_{-0.2}$	$7^{+1019}_{-0.1}$	$0.6^{+0.07}_{-0.3}$	13:01:26.56	29:17:39.4
TDG3p	8^{+420}_{-7}	$0.01^{+0.2}$	$0.05^{+0.07}_{-0.05}$	$2 \times 10^{3+1 \times 10^4}_{-1 \times 10^3}$	$0.2^{+0.3}_{-0.2}$	13:01:25.79	29:17:07.5
NUV1p	$5^{+0.2}_{-4}$	$100.^{-94.4}$	$0.6^{+0.06}_{-0.5}$	5^{+123}_{-4}	$0.6^{+0.06}_{-0.5}$	13:01:26.47	29:17:10.5
NUV2p	$19^{+5.4}_{-4.1}$	$9.^{+91}_{-6}$	$0.45^{+0.14}_{-0.32}$	40^{+101}_{-37}	$0.35^{+0.35}_{-0.11}$	13:01:26.97	29:17:21.5
NUV3p	200^{+363}_{-110}	$2.5^{+5.5}_{-1.5}$	$0.005^{+0.6}_{-0.005}$	6^{+1051}_{-5}	$0.6^{+0.1}_{-0.6}$	13:01:26.97	29:17:36.5

TABLE 2

APERTURE PHOTOMETRY MODELING RESULTS FOR “TDG1” AND “NUV1”

ID	$t_{YC,2CM}$ (Myr)	f_{YC} (%)	$E(B - V)_{2CM}$	M_{2CM} (M_{\odot})	t_{SSP} (Myr)	$E(B - V)_{SSP}$	M_{SSP} (M_{\odot})
TDG1+NUV1	4^{+1}_{-3}	$20.^{+80}_{-17}$	$0.3^{+0.01}_{-0.1}$	4.3×10^6	3^{+3}_{-2}	$0.3^{+0.01}_{-0.1}$	9.3×10^5
TDG1	$5^{+0.07}_{-4}$	$1.2^{+1.8}_{-0.29}$	$0.16^{+0.024}_{-0.028}$	3.1×10^7	$12^{+1.2}_{-11}$	$0.09^{+0.1}_{-0.08}$	1.1×10^6
NUV1	$5^{+0.06}_{-4}$	$7.^{+93}_{-5}$	$0.09^{+0.03}_{-0.03}$	3.4×10^6	$5^{+0.06}_{-4}$	$0.1^{+0.03}_{-0.03}$	3.8×10^5

for those two objects. In the case of “TDG1”, its UV light is blended with “NUV1” and we can see a faint optical counterpart for “NUV1” (the inset image in the right panel of Figure 1). Both of them show very blue optical colors ($g - r = 0.12$ and -0.26 for “TDG1” and “NUV1,” respectively). In fact, the pixel-by-pixel analysis in Section 4.1 showed that “NUV1p” has significantly younger stellar populations (~ 5 Myr) than “TDG1p” (~ 200 Myr). “NUV1” might be significantly contaminating the UV fluxes of its surrounding regions. Hence, we can not assume that “TDG1” is the sole optical counterpart of the brightest UV blob at the tip of the tidal tail.

Since it was impossible to deblend the UV lights between “TDG1” and “NUV1” at the tip of the tail, we integrated the optical SEDs from both objects in order to match the UV SED. We measured aperture magnitudes of “TDG1” and “NUV1” with an aperture size, $3 \times \text{FWHM}$ in the SDSS data. Also a magnitude of the corresponding UV blob was measured with an aperture of $3 \times \text{FWHM}$ from the *GALEX* data. We investigated stellar populations with three kind of SEDs

as “TDG1+NUV1,” “TDG1,” and “NUV1” for comparison.

The results of stellar population modeling are presented in Table 2. Figure 6 shows the best fits and χ^2 contours for three cases. The modeling suggests that “TDG1+NUV1” has a young stellar population about a few Myr old, contributing a substantial mass fraction up to 100 per cent with considerable internal extinction of $E(B - V) = 0.3$ mag. If we consider “TDG1” and “NUV1” separately, they show the existence of young stellar population of a few Myr old. In all two-component modeling cases the best fits were found when $t_{OC} = 12$ Gyr. The SSP fits suggest similar results, albeit for larger χ^2 than from two-component fits.

The stellar mass of this system is derived from the V -band luminosity estimated from the r -band luminosity using a transformation equation extracted from Jordi, Grebel & Ammon (2006). According to stellar population modeling, the mass of “TDG1+NUV1” system was estimated as $4.3 \times 10^6 M_{\odot}$ with two-component modeling and $9.2 \times 10^5 M_{\odot}$ with SSP modeling. Stellar masses of

“TDG1” and “NUV1” are also calculated separately based on their optical luminosities. Since the stellar mass-to-light ratio increases with the age of the stellar population, the mass of a young population derived by two-component fits is always greater than the mass estimate from SSP fits.

The use of the *GALEX* UV data played a critical role in the spectral fits. For example, Figure 7 shows that the best SSP models for “TDG1+NUV1” indicates the age of 3 Myr, while the fits without UV data lead to 16 Myr. While the χ^2 distributions for these two estimates are far from Gaussian, they are separated by 3σ at least. Recently, Hibbard et al. (2005) and Neff et al. (2005) have also demonstrated the ability of *GALEX* data to detect TDGs and to determine the age of young stellar populations (their estimates were based on SSP modeling using a UV color).

5. Summary

Tidal dwarf galaxies represent one of the possible progenitors of the general population of dwarf galaxies, featuring high metallicity and diverse star formation histories. In this paper we study the tidal tail around a post-merger galaxy, NGC 4922, in the Coma cluster. Combining UV and optical photometry, we discover a few TDG candidates in the tail. In our analysis, two-component models generally yield a better fit than SSP models for the tidal tail and TDG candidates, although young populations with a single age cannot be ruled out. Also TDG candidates showed a better fit with models with higher metallicity for a young component. According to the pixel-by-pixel and the aperture analyses, two optical TDG candidates and three NUV peaks show predominantly young stellar populations of a few Myr of age, suggesting that recent star formation occurred almost simultaneously along the tidal tail. The result also corresponds with the recent work on the interacting galaxy Arp 305 in which the age of TDG candidates was ~ 6 Myr (Hancock et al. 2009).

The pixel-by-pixel analysis adopted in this study is relatively new to the field. With the new deep and multiband photometric data, one can now perform statistically meaningful analyses pixel by pixel. A clear advantage of the pixel-by-

pixel analysis is that it allows us to make spatially resolved age maps, instead of estimates for an integrated region. Hence we can investigate the star formation history of the galaxy in connection with the merging event. The Coma cluster is a bit too far for such a detailed investigation. Closer cluster environments, such as Virgo and Fornax, provide better opportunities.

The UV data proved once again to be powerful for searching for young starbursts. The *GALEX* UV data on hundreds of nearby galaxies, mainly but not exclusively in the NGS survey mode, will provide other interesting opportunities without doubt.

Facilities: *GALEX*, SDSS, Perkins (PRISM)

We are indebted to Giuseppe Gavazzi and Alessandro Boselli for supporting our use of the *GALEX* data made public after their guest investigation acquired them but prior to their use. We thank the anonymous referee for various clarifications. This research was supported by Basic Science Research Program through the National Research Foundation of Korea (NRF) funded by the Ministry of Education, Science and Technology (Doyak 20090078756). S.K.Y. also acknowledges support from Korea Astronomy and Space Science Institute. We have used the *GALEX* UV data obtained from the Multimission Archive at the Space Telescope Science Institute (MAST). *GALEX* is operated for NASA by the California Institute of Technology under NASA contract NAS5-98034. We are grateful to the Lowell Observatory for granting observing time and hospitality during our visit.

REFERENCES

- Alonso-Herrero, A., Ward, M. J., Aragón-Salamanca, A., & Zamorano, J. 1999, *MNRAS*, 302, 561
- Andreasyan, N. K. & Khachikyan, É. E. 1986, *Astrophysics*, 24, 9
- Barnes, J. E. 1988, *ApJ*, 331, 699
- Barnes, J. E. & Hernquist, L. 1992, *Nature*, 360, 715
- Bertin, E. & Arnouts, S. 1996, *A&AS*, 117, 393

- Boquien, M., Duc, P.-A., Braine, J., Brinks, E., Lisenfeld, U., & Charmandaris, V. 2007, *A&A*, 467, 93
- Boquien, M., Duc, P.-A., Wu, Y., Charmandaris, V., Lisenfeld, U., Braine, J., Brinks, E., Iglesias-Páramo, J., & Xu, C. K. 2009, *AJ*, 137, 4561
- Bournaud, F. & Duc, P. -A. 2006, *A&A*, 456, 481
- Bournaud, F., Duc, P. -A. & Emsellem, E. 2008, *MNRAS*, 389, L8
- Calzetti, D. 2001, *PASP*, 113, 1449
- Cardelli, J. A., Clayton, G. C. & Mathis, J. S. 1989, *ApJ*, 345, 245
- Cortese, L, Gavazzi, G., & Boselli, A. 2008, *MNRAS*, 390, 1282
- Duc, P. -A., Brinks, E., Wink, J. E. & Mirabel, I. F. 1997, *A&A*, 326, 537
- Duc, P. -A. & Mirabel, I. F. 1998, *A&A*, 333, 813
- Duc, P. -A., Brinks, E., Springel, V., Pichardo, B., Weilbacher, P. & Mirabel, I. F. 2000, *AJ*, 120, 1238
- Elmegreen, B. G., Kaufman, M. & Thomasson, M. 1993, *ApJ*, 412, 90
- Ferreras, I. & Silk, J., 2000, *ApJ*, 541, L37
- Hancock, M., Smith, B. J., Struck, C., Giroux, M. L. & Hurlock, S. 2009, *AJ*, 137, 4643
- Heithausen, A. & Walter, F. 2000, *A&A*, 361, 500
- Hibbard, J. E., Guhathakurta, P., van Gorkom, J. H. & Schweizer, F. 1994, *AJ*, 107, 67
- Hibbard, J. E., van der Hulst, J. M., Barnes, J. E. & Rich, R. M. 2001, *AJ*, 122, 2969
- Hibbard, J. E. et al. 2005, *ApJ*, 619, L87
- Jordi, K., Grebel, E. K. & Ammon, K. 2006, *A&A*, 460, 339
- Kaviraj, S. et al. 2007, *ApJS*, 173, 619
- Konstantopoulos, I. S. 2009, arXiv:0909.0040
- Koribalski, B. S., & López-Sánchez, Á. R., *MNRAS*, in press (arXiv:0908.4128)
- Leitherer, C. et al. 1999, *ApJS*, 123, 3
- Martin D. C. et al., 2005, *ApJ*, 619, L1
- Mendes de Oliveira, C., Plana, H., Amram, P., Balkowski, C. & Bolte, M. 2001, *AJ*, 121, 2524
- Mirabel, I. F., Lutz, D. & Maza, J. 1991, *A&A*, 243, 367
- Mirabel, I. F., Dottori, H. & Lutz, D. 1992, *A&A*, 256, L19
- Morrissey et al. 2007, *ApJS*, 173, 682
- Mundell C. G., James, P. A., Loiseau, N., Schinnerer, E. & Firbes, D. A. 2004, *ApJ*, 614, 648
- Neff, S. G. et al. 2005, *ApJ*, 619, L91
- Recchi, S., Theis, C., Kroupa, P. & Hensler, G. 2007, *A&A*, 470, 5
- Ree, C. H. et al. 2007, *ApJS*, 173, 607
- Schlegel D. J., Finkbeiner D. P., Davis M., 1998, *ApJ*, 500, 525
- Schombert, J. M., Wallin, J. F. & Struck-Marcell, C. 1990, *AJ*, 99, 497
- Schweizer 1978, *IAUS*, 77, 279
- Smith, B. J., Giroux, M. L., Struck, C., Hancock, M. & Hurlock, S. 2009, arXiv:0908.3657
- Temporin, S., Weinberger, R., Galaz, G. & Kerber, F. 2003, *ApJ*, 587, 660
- Toomre, A. & Toomre, J, 1972, *ApJ*, 178, 623
- Wallin, J. F. 1990, *AJ*, 100, 1477
- Weilbacher, P. M., Duc, P. -A., Fritze von Alvensleben, U., Martin, P. & Fricke, K. J. 2000, *A&A*, 358, 819
- Weilbacher, P. M., Duc, P. -A. & Fritze-v. Alvensleben, U. 2003, *A&A*, 397, 545
- Wetzstein, M., Naab, T. & Burkert, A. 2007, *MNRAS*, 375, 80
- Yi, S. K. 2003, *ApJ*, 582, 202
- Yi, S. K. et al. 2005, *ApJ*, 619, L111
- York, D. G. et al. 2000, *AJ*, 120, 1579

Yoshida, M., Taniguchi, Y. & Murayama, T 1994,
PASJ, 46, L195

Zwicky 1956, Ergebnisse der exakten Naturwis-
senschaften, 29, 344